

Article

Numerical Evaluation of the Effect of Buoyancy-Driven Flow on the Migration of Respiratory Droplets

Nan Li ¹ and Xiaohong Yan ^{2,*}¹ Department of Nursing, Xi'an Jiaotong University City College, Xi'an 710018, China; linanxjtu@126.com² Shaanxi Key Laboratory of Energy Chemical Process Intensification, Department of Chemical Engineering, Xi'an Jiaotong University, Xi'an 710049, China

* Correspondence: xhyan11@mail.xjtu.edu.cn; Tel./Fax: +86-29-82665836

Abstract: The understanding of the impact of buoyancy-driven flow on the migration of respiratory droplets remains limited. To investigate this phenomenon, the Lagrangian–Eulerian approach (k- ϵ turbulent model and discrete phase model) was employed to analyze the interaction between buoyancy-driven flow and coughing activity. The simulation approach was validated by simulating a jet problem in water. Although this problem describes the jet penetration in water, the governing equations for this problem are the same as those for coughing activity in the air. The results demonstrated that an umbrella-shaped airflow was generated above a person and a temperature stratification existed in the room. The buoyancy-driven flow significantly altered the dispersion pattern of the droplets. Notably, for large droplets with an initial diameter of 100 μm , the flow in the boundary layer led to an increased deposition time by about five times. Conversely, for small droplets with an initial diameter of 20 μm , the umbrella-shaped airflow resulted in a more rapid dispersion of droplets and subsequently facilitated their quicker removal by the room walls. After a duration of 300 s, the suspended droplet number of the case with buoyancy-driven flow was 33.4% smaller than that of the case without buoyancy-driven flow. Two or three persons being in the room resulted in a faster droplet removal.

Keywords: respiratory droplet; dispersion; buoyancy; indoor; simulation

Citation: Li, N.; Yan, X. Numerical Evaluation of the Effect of Buoyancy-Driven Flow on the Migration of Respiratory Droplets. *Processes* **2023**, *11*, 2596. <https://doi.org/10.3390/pr11092596>

Academic Editors: Jose C. Merchuk and Yongping Chen

Received: 30 June 2023

Revised: 11 August 2023

Accepted: 28 August 2023

Published: 30 August 2023



Copyright: © 2023 by the authors. Licensee MDPI, Basel, Switzerland. This article is an open access article distributed under the terms and conditions of the Creative Commons Attribution (CC BY) license (<https://creativecommons.org/licenses/by/4.0/>).

1. Introduction

Airborne transmission is now considered to be one main transmission routes of respiratory viruses, such as COVID-19 [1,2]. Droplets are produced by various expiratory activities, such as the speaking and coughing of an infected person [3]. These droplets may be suspended in the air for a long time. The lifetime for droplets with a diameter of 5 μm may be about 33 min [2] and infection may occur when the suspended droplets are inhaled by a person. Understanding the migration behavior of droplets is important to controlling the spread of respiratory viruses.

The diameter and number of respiratory droplets depend on the expiratory activities [4,5]. The number and geometric mean diameter of the droplets expelled by per cough are about 947 to 2085 and 13.5 μm , respectively [4]. The respiratory droplet is usually considered as a non-evaporative nuclei covered with a layer of water and the mass fraction of the water is about 94% [6]. The migration of respiratory droplets depends on the air stream generated by the expiratory activity, temperature, humidity, and flow pattern of the ambient air. The transient velocity profiles of different expiratory activity are different. The average expiration air velocities for coughing and speaking are 11.7 m s^{-1} and 3.9 m s^{-1} , respectively [4]. The duration time of coughing is usually less than 1 s. The jet-like flow pattern is generated during the speaking [3]. In an indoor environment without ventilation, the migration of droplets depends on the air stream generated by the expiratory activity. When ventilation in the indoor environment or wind in the outdoor environment exists, the droplet migration highly depends on the ventilation [7,8] or wind [9,10].

Evaporation significantly influences the migration of respiratory droplets [11]. The evaporation of a respiratory droplet is different from the water droplet due to the non-evaporative nuclei [11]. Large droplets may change to small particles (with a diameter of about 20% [12] or 32% [13] of the initial diameter) during the migration process and be suspended in the air for a long time. Small droplets (diameter $\leq 12 \mu\text{m}$) generated by coughing may travel 4 m away along the streamwise direction [6]. The droplet evaporation rate depends on the temperature and humidity of the ambient air [14–16]. It is reported that the evaporation is diffusion-limited when the droplet radius is in the range of 70 nm to 60 μm [14]. The migration process of respiratory droplets is vital for the understanding of the transmission of respiratory viruses.

The computational fluid dynamics (CFD) simulation is widely used to predict the migration process of respiratory droplets. The capabilities and limitations of airborne and aerosol pathogen CFD modeling were discussed in Sheikhejad et al. [17]. For the transport process involving two phases (air and discrete droplets), there are two types of simulation approaches: the Eulerian–Eulerian approach and Lagrangian–Eulerian approach. The Lagrangian–Eulerian approach was reported to be better at predicting the transient dispersion of the particles [18]. For the turbulent flow of air, the RNG $k-\varepsilon$ model was reported to provide reasonable accuracy and stability [19]. For the droplet migration process, the collision between droplets is usually neglected due to the low probability of collision in typical indoor environments with a low volume fraction of respiratory droplets [17]. The CFD simulation requires many parameters gained from experimental measurements, such as the droplet size and velocity of the respiratory activity. The predictive accuracy of the CFD simulation depends on the collected data [17].

In typical indoor environments, an obvious temperature difference between a person and the air exists, which may lead to the buoyancy-driven flow (the thermal plume). The buoyancy-driven flow forms a human microenvironment in the region near a person. An experimental investigation [20] demonstrated that the thermal plume depended on many factors, such as body structures and types of clothing. Recently, the thermal plume generated by a person was simulated and the variation of the droplet concentration was predicted by an inert scalar equation [21]. The migration of individual droplets was not directly simulated. The thermal plume and the effect of thermal plume on droplet migration was recently reviewed by Sun et al. [22]. They pointed out that the influences of human thermal plumes on droplet migration in the human boundary layer have been barely investigated and the droplet migration in the human microenvironment is an important knowledge gap.

To our best knowledge, the effect of buoyancy-driven flow on the dynamic variation of the number of suspended droplets is poorly understood. Hence, the objective of the current study is to numerically discuss the flow pattern of buoyancy-driven flow and the effect of the flow on the dynamic variation of the number of suspended droplets.

2. Physical Problems

Two problems widely investigated by the researchers were first simulated in this study to evaluate the accuracy of the current simulation method. Then, the problems of buoyancy-driven flow and droplet migration in a room were simulated.

2.1. Validation Problem 1: Jet Penetration

Previous research investigated the dispersion of food dye in a water tank and the dye penetration length was recorded as a function of time [23], as shown in Figure 1. The food dye was injected from a nozzle with a diameter of 10 mm. The size of the water tank was 1.5 m (x) \times 1 m (y) \times 1.2 m (z). The height of the water level and the center of the nozzle were 1 m and 0.5 m, respectively. The streamwise penetration depth was evaluated according to the recorded photo, as shown in Figure 1b. The time-dependent velocity profile at the nozzle exit was similar to a real-cough profile, which is shown in Figure 2. The velocity profile was fitted by a polynomial expression and applied in the current simulation.

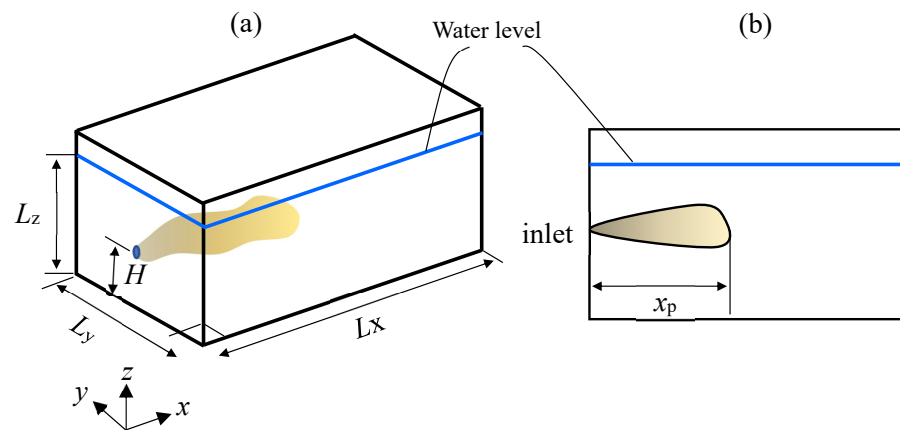


Figure 1. Description of (a) the penetration of a jet in water and (b) the determination of the penetration depth from the velocity contour.

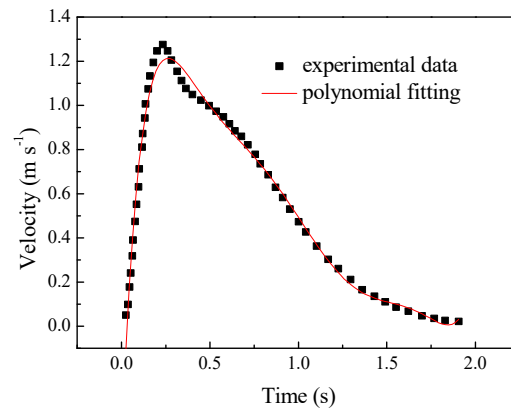


Figure 2. The time-dependent velocity at the inlet was similar to a human cough jet.

The problem was simulated to evaluate the prediction accuracy of cough flow. In the simulation, the three-dimensional geometry and velocity profile were the same as that in the experiment. The velocity contours at various moments were analyzed to evaluate the jet penetration depth.

2.2. Validation Problem 2: Droplet Evaporation

The evaporation of a water droplet in an air stream was experimentally investigated [24] and the variation of the droplet diameter was measured. A droplet with an initial diameter of 1.2 mm was hung on a wire in a rectangular channel. The two-dimensional problem is schematically described in Figure 3. The characteristic size of the channel was 70 mm. An air stream entered the channel with a velocity of 0.203 m s^{-1} . The temperature and relative humidity of the air were $24 \text{ }^\circ\text{C}$ and 35%, respectively.

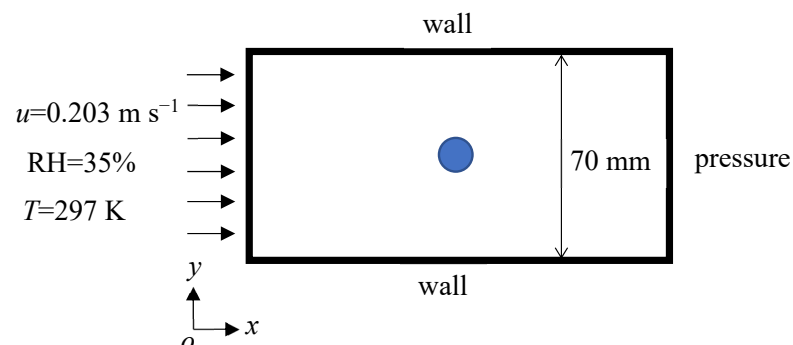


Figure 3. Description of the droplet evaporation problem.

The problem was simulated to evaluate the prediction accuracy of droplet evaporation. In the simulation, the wire was not considered because detailed information about the wire was not provided in the experimental literature.

2.3. Buoyancy-Driven Flow and the Cough Problem

The droplet migration process in an indoor environment was analyzed and the geometry is shown in Figure 4. The size of the room was 5 m (x) \times 5 m (y) \times 3 m (z). A column with a size of 0.5 m (x) \times 0.5 m (y) \times 1.8 m (z) located in the center of the room was used to approximate a person. Droplets were injected from a circular plane located at the surface of the column. The circular plane was similar to the mouth of a person and the diameter of the circular plane was 21 mm [6]. The height of the center of the circular plane was 1.7 m [6]. The geometry was symmetric; hence, half of the geometry was used as the computational domain (three-dimensional) with the symmetry boundary. In order to investigate the effect of person number in the room, two other cases with two or three columns with a spacing of 1.25 m along the y -axis were constructed, as shown in Figure 4b,c. Meshes were generated and the sensitivity of the simulation results to the mesh number was evaluated to obtain mesh-independent results. The meshes in the symmetry plane are shown in Figure 5.

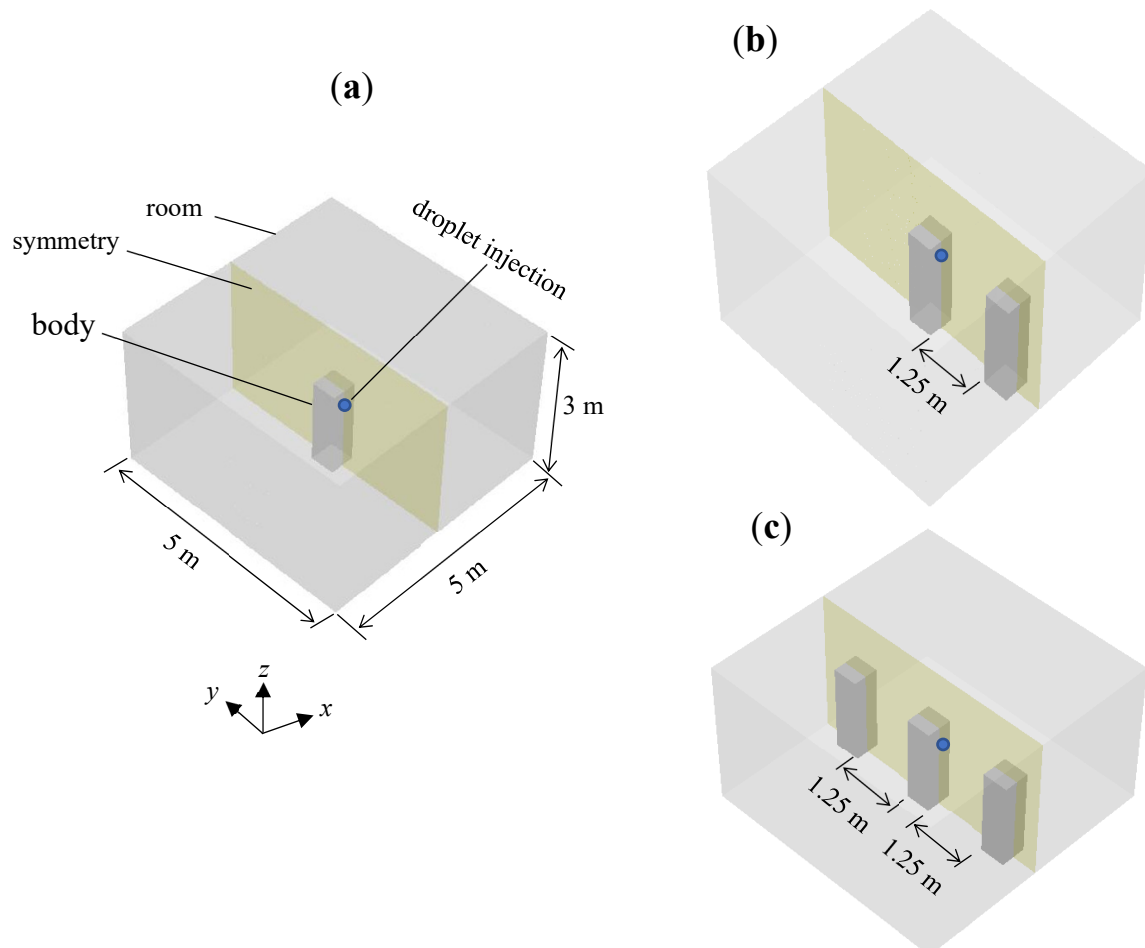


Figure 4. Geometry of the respiratory droplets migration problem. (a) one column. (b) two columns. (c) three columns.

A transient simulation was conducted. Initially, the air in the room was still and the temperature and relative humidity were 20 °C and 50%, respectively. The temperature of all walls of the room was 20 °C. Air was treated as an ideal gas. The time-dependent velocity profile [6] at the circular plane is shown in Figure 6, with a duration time of 0.61 s. The air stream injected from the circular plane had a temperature of 35 °C. The relative

humidity was assumed to be 100%. Droplets with the same temperature as the air stream were injected into the room during a time span of 0.61 s. The droplet injection time interval was 0.03 s and the injection number was about 900 during the cough time period. The emitted droplet number was in the range reported in [4]. The effect of droplet diameter was discussed for two different values, 20 μm and 100 μm . The mass flow rate of droplets was evaluated according to the droplet number, diameter, and injection time. Droplets were considered trapped when droplets collided with the walls. The two-way coupling method was used in the simulation, which demonstrated that the air flow influences the migration of droplets and the migration of droplets also influences the airflow. The contribution of turbulent dispersion to droplet migration was considered by the discrete random walk approach in ANSYS-Fluent [25]. The simulation was conducted with various timesteps ranging from 0.0001s to 0.05 s. The convergence criteria in each timestep were 10^{-6} for energy and 10^{-3} for other parameters.

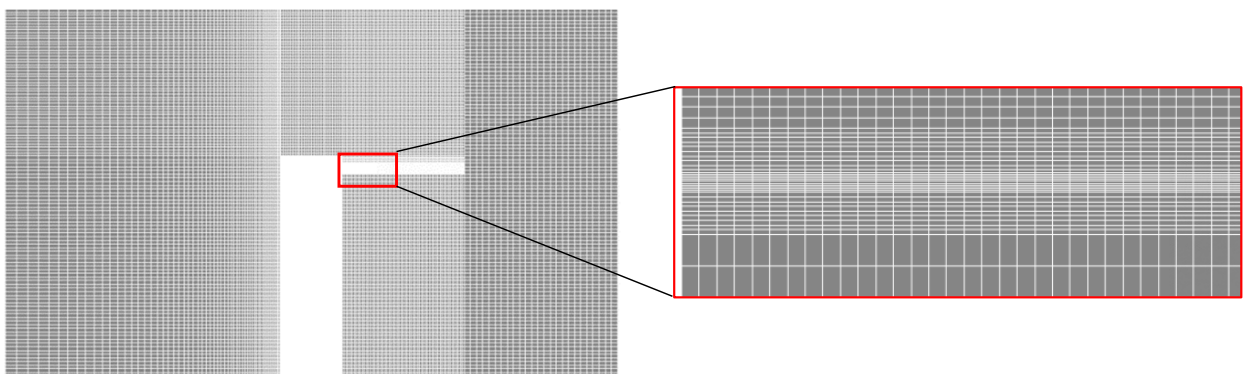


Figure 5. Meshes in the symmetry plane.

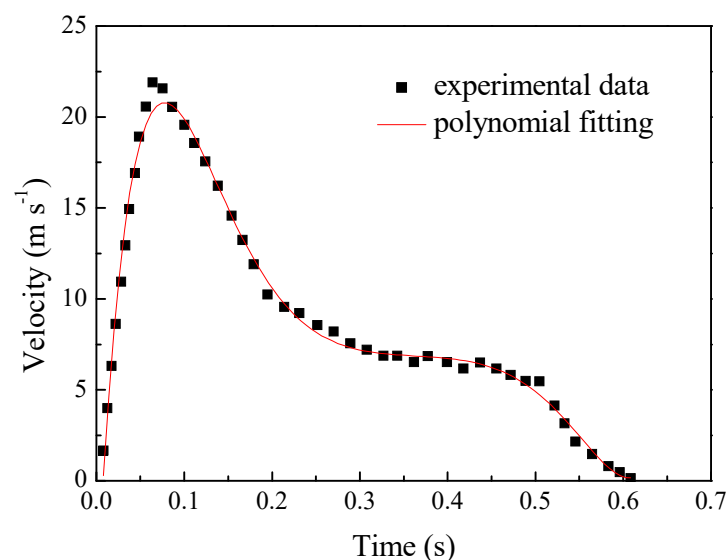


Figure 6. Velocity profile of a cough flow.

3. Numerical Models

To predict the migration behavior of respiratory droplets, four sub-models are required: (1) momentum transfer caused by the expiratory activity and buoyancy force, (2) heat transfer due to the temperature difference between the air stream generated by a person and the ambient air, (3) species transfer due to the droplet evaporation and (4) the droplet migration. These sub-models interact with each other and should be solved simultaneously. The respiratory droplet migration process is similar to the process described in our previous research under the condition without corona discharge [26].

Some approximations in the current simulations are:

- Droplets were treated as spherical droplets;
- Droplet collision was negligible due to the small volume fraction of droplets in the air;
- The Stefan flow was neglected due to the small temperature difference between the respiratory droplets and the ambient air [27];
- The density of the respiratory droplets is approximated to be the same as that of water droplets due to the high mass fraction of water in typical respiratory droplets [6];
- The person is approximated as a column with a uniform temperature of 35 °C.

The mathematical models were solved by the software ANSYS-Fluent and some user-defined functions. The two-phase transport process was simulated by the Lagrangian–Eulerian approach to obtain better prediction accuracy of the transient droplet migration process [18]. The transient turbulent flow was simulated by the k - ε model with the enhanced wall treatment. The k - ε model provided reasonable accuracy and stability for predicting expiratory activities, as discussed in the previous literature [19]. A two-way coupling discrete phase model (DPM) was used to predict the transient droplet migration. Droplet evaporation was simulated by the diffusion-controlled model. For each case, mesh sensitivity was evaluated to obtain mesh-independent results.

3.1. Continuous Phase Model

1. Gas flow

The gas flow is solved by the k - ε model in ANSYS-Fluent. The mass and momentum exchanges between the droplets and gas respectively appear as the mass and momentum sources in the continuity equation and the momentum equation. The gas flow is considered a steady flow of the incompressible ideal gas due to the low gas velocity (no more than 2 m/s), which can be solved by:

$$\frac{\partial \rho}{\partial t} + \nabla \cdot (\rho \mathbf{u}_{\text{gas}}) = S_m \quad (1)$$

$$\frac{\partial}{\partial t} (\rho \mathbf{u}_{\text{gas}}) + \rho \mathbf{u}_{\text{gas}} \cdot \nabla \mathbf{u}_{\text{gas}} = -\nabla P + (\mu + \mu_t) \nabla^2 \mathbf{u}_{\text{gas}} + \rho \mathbf{g} + \mathbf{F} \quad (2)$$

$$\frac{\partial}{\partial t} (\rho k) + \rho \mathbf{u}_{\text{gas}} \cdot \nabla k = \nabla \cdot \left(\left(\mu + \frac{\mu_t}{\sigma_k} \right) \nabla k \right) - \rho \varepsilon + \mu_t \left[\nabla \mathbf{u}_{\text{gas}} : \left(\nabla \mathbf{u}_{\text{gas}} + (\nabla \mathbf{u}_{\text{gas}})^T \right) \right] \quad (3)$$

$$\frac{\partial}{\partial t} (\rho \varepsilon) + \rho \mathbf{u}_{\text{gas}} \cdot \nabla \varepsilon = \nabla \cdot \left(\left(\mu + \frac{\mu_t}{\sigma_\varepsilon} \right) \nabla \varepsilon \right) + C_{\varepsilon 1} \frac{\varepsilon}{k} \mu_t \left[\nabla \mathbf{u}_{\text{gas}} : \left(\nabla \mathbf{u}_{\text{gas}} + (\nabla \mathbf{u}_{\text{gas}})^T \right) \right] - C_{\varepsilon 2} \frac{\varepsilon^2}{k} \quad (4)$$

$$\mu_t = \rho c_\mu \frac{k^2}{\varepsilon} \quad (5)$$

where μ and μ_t are the gas viscosity and turbulence viscosity, respectively; k and ε are the turbulent kinetic energy and turbulent rate of dissipation, respectively; $C_{\varepsilon 1}$, $C_{\varepsilon 2}$, c_μ , σ_k , and σ_ε are model constants and the default values in ANSYS-Fluent are applied. S_m represents the mass source term caused by the evaporation of the droplets and \mathbf{F} is the force on the gas exerted by droplets:

$$S_m = \frac{\sum_{n=1}^N \frac{m_{s,0}}{m_{d,0}} \Delta t_n \Delta m_d}{V_{\text{cell}}} \quad (6)$$

$$\mathbf{F} = \left(\sum_{n=1}^N \frac{m_{s,0}}{m_{d,0}} \Delta t_n m_d \frac{18\mu}{\rho_d d_d^2} \frac{C_d Re}{24} (\mathbf{u}_d - \mathbf{u}_{\text{gas}}) \right) / V_{\text{cell}} \quad (7)$$

where Δm_d represents the change of droplet mass per second. C_d is the drag coefficient [28] and Re is the relative Reynolds number:

$$Re = (\rho_d d |\mathbf{u}_{\text{gas}} - \mathbf{u}_d|) / \mu \quad (8)$$

- Heat transfer

The heat transfer during the flow of the airstream generated by the respiratory activity is simulated by solving the energy conservation equation. The energy conservation equation for the steady flow can be expressed as:

$$\frac{\partial}{\partial t} (\rho h_g) + \nabla \cdot (\mathbf{u}_{\text{gas}} \rho h_g) = \nabla \cdot \left((k_h + k_{h,t}) \nabla T - \sum_{i=1}^j h_i \mathbf{J}_i + \mu \mathbf{u}_{\text{gas}} \cdot \nabla \mathbf{u}_{\text{gas}} \right) + S_e \quad (9)$$

where h_g is the specific enthalpy of the gas mixture; k_h and $k_{h,t}$ are the gas thermal conductivity and the turbulent thermal conductivity, respectively; h_i is the sensible enthalpy of species i and \mathbf{J}_i is the mass diffusion flux of species i , whose expression can be referred to Equation (12); S_e is the energy source term caused by the energy exchange between the droplets and gas, which can be computed as:

$$S_e = \frac{\sum_{s=1}^S \frac{m_{s,0}}{m_{d,0}} (m_{d,\text{in}} h_{d,\text{in}} - m_{d,\text{out}} h_{d,\text{out}} - (m_{d,\text{in}} - m_{d,\text{out}}) h_{\text{lat}})}{V_{\text{cell}}} \quad (10)$$

where s is the number of droplet streams in one cell; $m_{d,\text{in}}$ and $m_{d,\text{out}}$ are the droplet mass at the entrance and exit of the current cell, respectively; $h_{d,\text{in}}$ and $h_{d,\text{out}}$ are the sensible enthalpy of the droplets at the entrance and exit of the current cell, respectively; h_{lat} is the latent heat of droplet evaporation.

- Species transfer

The species transfer and mass fraction distribution of the water vapor can be solved by the following expression:

$$\frac{\partial}{\partial t} (\rho Y_v) + \nabla \cdot (\rho Y_v \mathbf{u}_{\text{gas}}) = -\nabla \cdot \mathbf{J}_v + S_v \quad (11)$$

where Y_v is the local mass fraction of water vapor; \mathbf{J}_v is the mass diffusion flux of water vapor; S_v represents the generation rate of water vapor caused by droplet evaporation:

$$\mathbf{J}_v = -(\rho D_{v,m} + \rho D_t) \nabla Y_v \quad (12)$$

$$S_v = \frac{\sum_{n=1}^N \frac{m_{s,0}}{m_{d,0}} \Delta t_n \Delta m_d}{V_{\text{cell}}} \quad (13)$$

where $D_{v,m}$ and D_t are the mass diffusion coefficient and turbulent diffusion coefficient of water vapor in the gas mixture, respectively.

3.2. Discrete Phase Model

- Droplet migration

The migration of droplets can be solved by the discrete particle model (DPM) in ANSYS-Fluent, which tracks the droplet trajectories by equating the droplet inertia with the sum of the forces acting on the droplet:

$$\frac{d\mathbf{u}_d}{dt} = \frac{18\mu}{\rho_d d^2} \frac{C_d Re}{24} (\mathbf{u}_{\text{gas}} - \mathbf{u}_d) + \frac{\mathbf{g}(\rho_d - \rho)}{\rho_d} \quad (14)$$

where the right two terms of Equation (14) represent the gas drag force and buoyancy force, respectively.

- Droplet heating and evaporation

The heating and evaporation processes of the droplets can also be solved by the DPM. The evaporation rate of a droplet depends on the difference between the water vapor concentration at the droplet surface and that in the bulk gas, which can be expressed by:

$$\frac{dm_d}{dt} = k_m A_d M_v (C_{v,s} - C_{v,\infty}) \quad (15)$$

where k_m is the mass transfer coefficient; A_d is the surface area of the droplet; M_v is the molecular weight of water vapor; $C_{v,s}$ and $C_{v,\infty}$ are the mole concentration of the water vapor at the droplet surface and in the bulk gas respectively, which can be calculated as:

$$C_{v,s} = \frac{P_{\text{sat}}(T_d)}{RT_d} \quad (16)$$

$$C_{v,\infty} = X_{v,\infty} \frac{P_\infty}{RT_\infty} \quad (17)$$

where T_d is the temperature of the droplet; $P_{\text{sat}}(T_d)$ is the saturated vapor pressure at T_d ; R is the universal gas constant; $X_{v,\infty}$, P_∞ , and T_∞ are the vapor mole fraction, pressure, and temperature of local bulk gas.

The change in the droplet temperature can be calculated by:

$$m_d c_{p,d} \frac{dT_d}{dt} = h A_d (T_\infty - T_d) - \frac{dm_d}{dt} h_{\text{lat}} \quad (18)$$

where $c_{p,d}$ is the specific heat capacity of the droplet and h is the convective heat transfer coefficient. The right two terms of Equation (18), respectively, represent the convective heat transfer between the droplet and gas and the latent heat required for droplet evaporation.

The mass transfer coefficient k_m in Equation (15) and convective heat transfer coefficient h in Equation (18) are calculated according to the expressions of the Sherwood number Sh and Nusselt number Nu [29,30], respectively:

$$Sh = \frac{k_m d_d}{D_{v,m}} = 2.0 + 0.6 Re^{1/2} Sc^{1/3} \quad (19)$$

$$Sc = \frac{\mu}{\rho D_{v,m}} \quad (20)$$

$$Nu = \frac{h d_d}{k_h} = 2.0 + 0.6 Re^{1/2} Pr^{1/3} \quad (21)$$

$$Pr = \frac{c_p \mu}{k_h} \quad (22)$$

where Sc and Pr are the Schmidt number and the Prandtl number of the continuous phase, respectively, and c_p is the heat capacity of the gas.

4. Results and Discussion

4.1. Model Validation

4.1.1. Jet Penetration Validation

The jet penetration problem described in Section 3.1 was simulated and the penetration depth was evaluated according to the velocity contour. Figure 7a shows the velocity contour in the slice ($y = L_y/2$) at the moment of 1.0 s. The penetration depth as a function of time

was evaluated and compared with the experimental data in Figure 7b. The characteristic velocity of the injection and Reynolds number were defined as:

$$U_c = \frac{1}{\Delta t} \int_0^{\Delta t} U(t) dt, \quad \text{Re} = \frac{\rho U_c D}{\mu} \quad (23)$$

where Δt and D are the duration time of the injection (0.61 s) and diameter of the circular plane, respectively. U_c and Re are 0.52 m s^{-1} and 5200, respectively. The sensitivity of the mesh number to the penetration depth is shown in Figure 7b, which demonstrates that nearly-mesh-independent results are obtained when the mesh number is more than 1.25 million. The sensitivity of the time step to the penetration depth is also shown in Figure 7b, which demonstrates that the results are insensitive to the time step when the time step is less than 0.01 s for this jet penetration problem. The sensitivities of the mesh size and time step to the results were also evaluated for other problems investigated in this study. The predicted penetration depth agrees well with the experimental data, demonstrating the good accuracy of cough flow prediction. Although this problem describes the jet penetration in water, the governing equations for this problem are the same as those for the coughing activity in the air. Therefore, experimental data for this problem can be used to evaluate the accuracy of predicting the coughing activity [6].

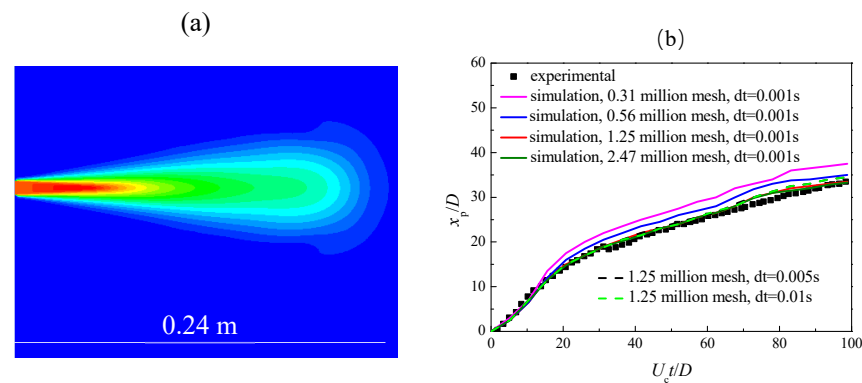


Figure 7. Simulation results of dye penetration. (a) The velocity contour at $t = 1.0$ s and (b) the normalized penetration depth as a function of the normalized time.

4.1.2. Droplet Evaporation Validation

The droplet evaporation problem described in Section 3.2 was simulated and the variation of droplet diameter with time is shown in Figure 8. The predicted diameter is less than the experimental data, with a normalized mean square error (NMSE) of 0.0023. The deviation may be caused by the neglect of the wire connected to the droplet. According to the criteria of a reasonable simulation [31], the current NSME is much less than 0.25. Hence, the droplet evaporation in the ambient air can be reasonably predicted by the numerical model described in Section 2.

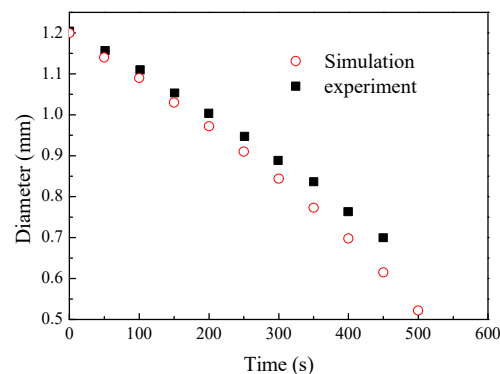


Figure 8. Droplet diameter variation due to evaporation.

4.2. Flow Pattern of the Buoyancy-Driven Flow

When persons stay in a room for some time, the temperature of the indoor air will change with time due to the temperature difference between the human body and the initial indoor air. The air density is sensitive to the air temperature and, accordingly, the nonuniform distribution of air density in the room leads to the buoyancy force. The buoyancy force can be expressed as $(\rho - \rho_0)g$; $\rho(\mathbf{r}, t)$ and $\rho_0(\mathbf{r}, t = 0)$ are the density of the air at a moment and the initial density, respectively. Hence, the buoyancy force will generate a flow even if no ventilation occurs in the room. The transient air flow and heat transfer processes were simulated and the results demonstrated that a steady state was obtained after about 300 s. In offices, wards, and classrooms, people usually stay for more than 300 s and a steady buoyancy-driven flow occurs. In the following sections, only the steady buoyancy-driven flow pattern is discussed.

Figure 9a,b show the air temperature contours at the symmetry plane. A temperature stratification can be observed and an upper layer above the column has an obviously higher temperature. Although the size of the column along the horizontal direction (y -axis in Figure 9) is one order of magnitude smaller than the size of the room, the air temperature in all of the upper layers of the room is influenced by the column. In the bottom layer, only a thin temperature boundary layer exists near the column and the boundary layer thickness increases vertically. Outside the temperature boundary layer, the air temperature remains the initial value. For the case with two columns, the temperature in the upper layer is higher. The air temperature in the region between two columns maintains the initial value. The nonuniform air temperature results in the nonuniform distribution of the air density. In the symmetry plane, the minimum and maximum densities are 1.16 and 1.21 kg m^{-3} , respectively. The upward buoyancy force is expected to exist in the region with a higher temperature and a lower air density.

The temperature field is coupled with the velocity field. Figure 9c,d show the velocity vectors at the symmetry plane. A thin velocity boundary layer exists near the column in the bottom layer, which is consistent with the thin temperature boundary layer. In the velocity boundary layer, the air flows upward and the air accelerates along the vertical direction. In the upper layer, the airflow with a characteristic size of about 0.5 m flows upward well above the column. When the airflow hits the ceiling of the room, the air flows tangentially along the ceiling. The airflow shows an umbrella shape. The order of magnitude of the air velocity is about 0.5 m s^{-1} . The tangential flow along the ceiling is the reason for the temperature stratification in Figure 9a,b. When two persons stand in the room, an obvious interaction occurs between these two airflows and a vortex exists, as shown in Figure 9d.

It is inferred that the buoyancy-driven flow depends on the initial temperature of the indoor air, which is qualitatively analyzed here. In a room with a lower temperature, the higher temperature difference between the human body and indoor air leads to a higher air density difference in the room. Accordingly, the buoyancy force is expected to be larger $((\rho - \rho_0)g)$ and the order of magnitude of the air velocity may be larger. In addition, if the person sits in the room, the region above the person is larger than the case with a person standing in the room, which will result in a more significant influence of the buoyancy-driven flow on the indoor airflow. Hence, the buoyancy-driven flow pattern is expected to be sensitive to the number and distribution shape of the persons in the room.

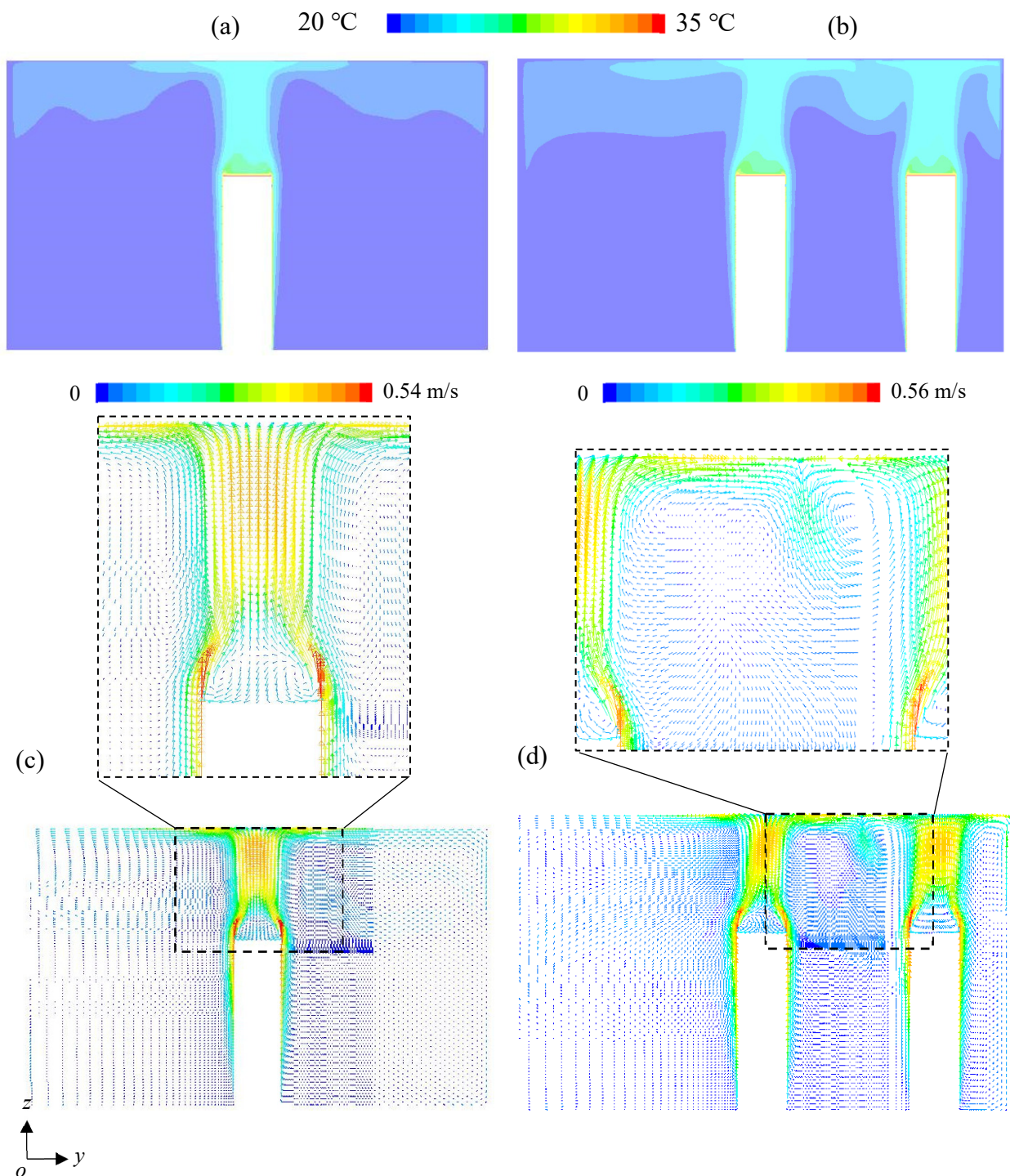


Figure 9. Temperature contours and velocity vectors at the symmetry plane. (a,c) for the case with one column and (b,d) for the case with two columns.

4.3. Respiratory Droplet Migration

When one infected person in the room coughs, a jet flow will be generated. Respiratory droplets will migrate with the jet flow. In order to discuss the effect of the buoyancy-driven flow on the droplet migration process, two cases under two different temperature conditions (20 °C and 35 °C) at the column's surfaces were simulated and compared. The dispersion of droplets with two different diameters (100 μm and 20 μm) was predicted. The jet flow velocity during the coughing activity (Figure 6) was much larger than the characteristic

velocity of the buoyancy-driven flow ($\sim 0.5 \text{ m s}^{-1}$). Hence, the droplet dispersion behavior was expected to be influenced by the jet flow during the initial stage. Figure 10a,c show the droplet dispersion patterns for the case without the buoyancy-driven flow (20°C at the column's surfaces, droplets with a diameter of $100 \mu\text{m}$) at two moments (0.8 s and 9 s). At the moment of 0.8 s, the distance between the front edge of the droplet cloud and the injection plane is about 1 m. The droplet diameter ranges from $95.1 \mu\text{m}$ to $98.8 \mu\text{m}$, which demonstrates the weak droplet evaporation. During the initial stage, the droplets migrate with the jet flow and the water vapor mass fraction in the jet flow is much larger than that in the ambient air. Hence, the droplet evaporation is weak. After the coughing activity terminates, no jet flow exists and the migration of droplets is dominated by the gravity force. At the moment of 9 s, the droplet cloud is near the floor and the droplet diameter ranges from $39.1 \mu\text{m}$ to $44.5 \mu\text{m}$. If the water in the respiratory droplet is thoroughly evaporated, the diameter of the droplet is $39.1 \mu\text{m}$. Hence, some droplets are thoroughly evaporated during the migration process. The number of droplets (droplets with a diameter of $100 \mu\text{m}$) suspended in the air as a function of time is shown in Figure 11, which demonstrates that all droplets are deposited on the floor in 30 s if the buoyancy-driven flow is not considered. Figure 10b,d show the droplet dispersion patterns for the case with buoyancy-driven flow (35°C at the column's surfaces, droplets with a diameter of $100 \mu\text{m}$). At the moment of 0.8 s, the droplet dispersion pattern is similar to the case without buoyancy-driven flow, which is reasonable because the droplet migration is dominated by the coughing activity during the initial stage. However, an obvious difference in the droplet dispersion patterns can be observed between cases without and with the buoyancy-driven flow at the moment of 9 s. Firstly, all droplets are thoroughly evaporated in Figure 10d, indicating that the buoyancy-driven flow enhanced the droplet evaporation. The droplet evaporation process is a convective mass transfer process and the airflow around the droplet enhances the evaporation process. As discussed in the above section, the buoyancy-driven flow disturbs the indoor air and, accordingly, enhances the droplet evaporation process. Secondly, some droplets are suspended in the region above the column and in the velocity boundary layer, which is consistent with the flow pattern shown in Figure 9. The upward flow exerts an upward drag force and, accordingly, inhibits the droplet deposition. The number of droplets suspended in the air as a function of time is shown in Figure 11. The droplet number (droplets with a diameter of $100 \mu\text{m}$) decreases fast before 30 s and there are about 3% of the droplets suspended in the air at the moment of 30 s. Further deposition of the suspended droplets is difficult and there are still 2% of the droplets suspended in the air at the moment of 250 s. If the deposition time is defined as the time when more than 99% of the droplets have been deposited on the walls of the room, then the buoyancy-driven flow near the column increases the droplet deposition time (with an initial diameter of $100 \mu\text{m}$) by about five times. The number of droplets (droplets with a diameter of $20 \mu\text{m}$) suspended in the air as a function of time is also shown in Figure 11 for comparison. The results demonstrate that the deposition of small droplets is difficult and the effect of buoyancy-driven flow on the deposition of small droplets is relatively weak. Under the condition with buoyancy-driven flow, the droplet number at the same time is smaller than that of the case under the condition without buoyancy-driven flow. After 300 s, the suspended droplet number of the case with buoyancy-driven flow is 33.4% smaller than that of the case without buoyancy-driven flow. For large droplets with a diameter of $100 \mu\text{m}$, droplets are captured by the floor of the room due to the deposition. For small droplets with a diameter of $20 \mu\text{m}$, droplets will be suspended in the air for more than 5 min. These small droplets may be captured by the floor and side walls of the room due to the turbulent dispersion. The buoyancy-driven flow increases the velocity of small droplets and, accordingly, this increases with the possibility of droplet collision with the walls of the room. When droplets collide with the walls of the room, droplets are captured. Hence, the buoyancy-driven flow slightly enhances the capture of small droplets. If the droplets contain a respiratory virus, the longer suspension time will increase the infection risk. Hence, the buoyancy-driven flow may increase the infection risk for persons in indoor environments.

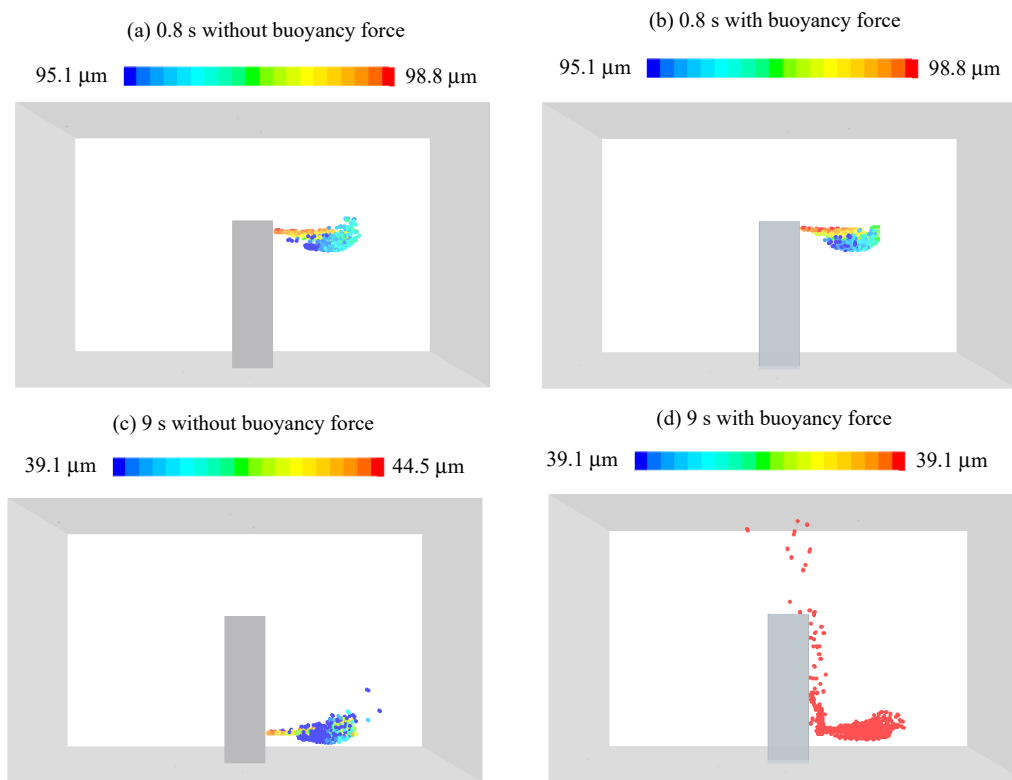


Figure 10. The droplet ($d = 100 \mu\text{m}$) dispersion pattern under the conditions (1) without buoyancy-driven flow and (2) with buoyancy-driven flow.

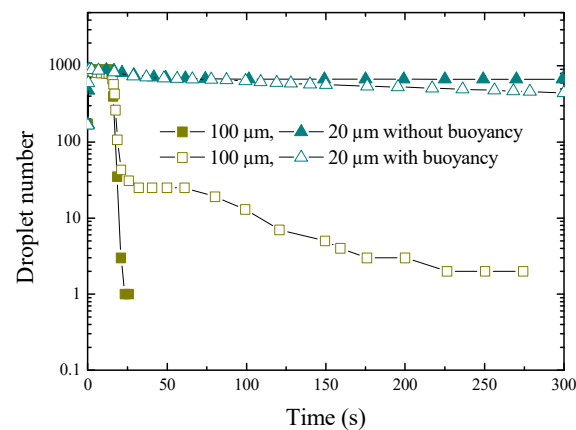


Figure 11. The number of droplets floating in the air as a function of the time.

Droplets generated by typical respiratory activities have a diameter ranging from several microns to several hundred microns. The forces on droplets with different diameters may be different and further influence the droplet dispersion behavior. Droplets with an initial diameter of $20 \mu\text{m}$ were injected and the dispersion patterns at different moments are shown in Figure 12. Figure 12a–d correspond to the case with one person in the room. Compared with the dispersion patterns in Figure 10, the droplets with a smaller diameter are more easily thoroughly evaporated and more difficult to deposit on the walls. At the moment of 2 s, the water in all droplets is thoroughly evaporated, which is reasonable for the large surface-to-volume ratio of smaller droplets. Most droplets are suspended in the air after 60 s and the droplets are mainly suspended in the downstream region of the jet flow. The number of droplets suspended in the air is plotted in Figure 13, which demonstrates that about 45% of the droplets are suspended in the air after 300 s, much larger than the number of droplets with an initial diameter of $100 \mu\text{m}$.

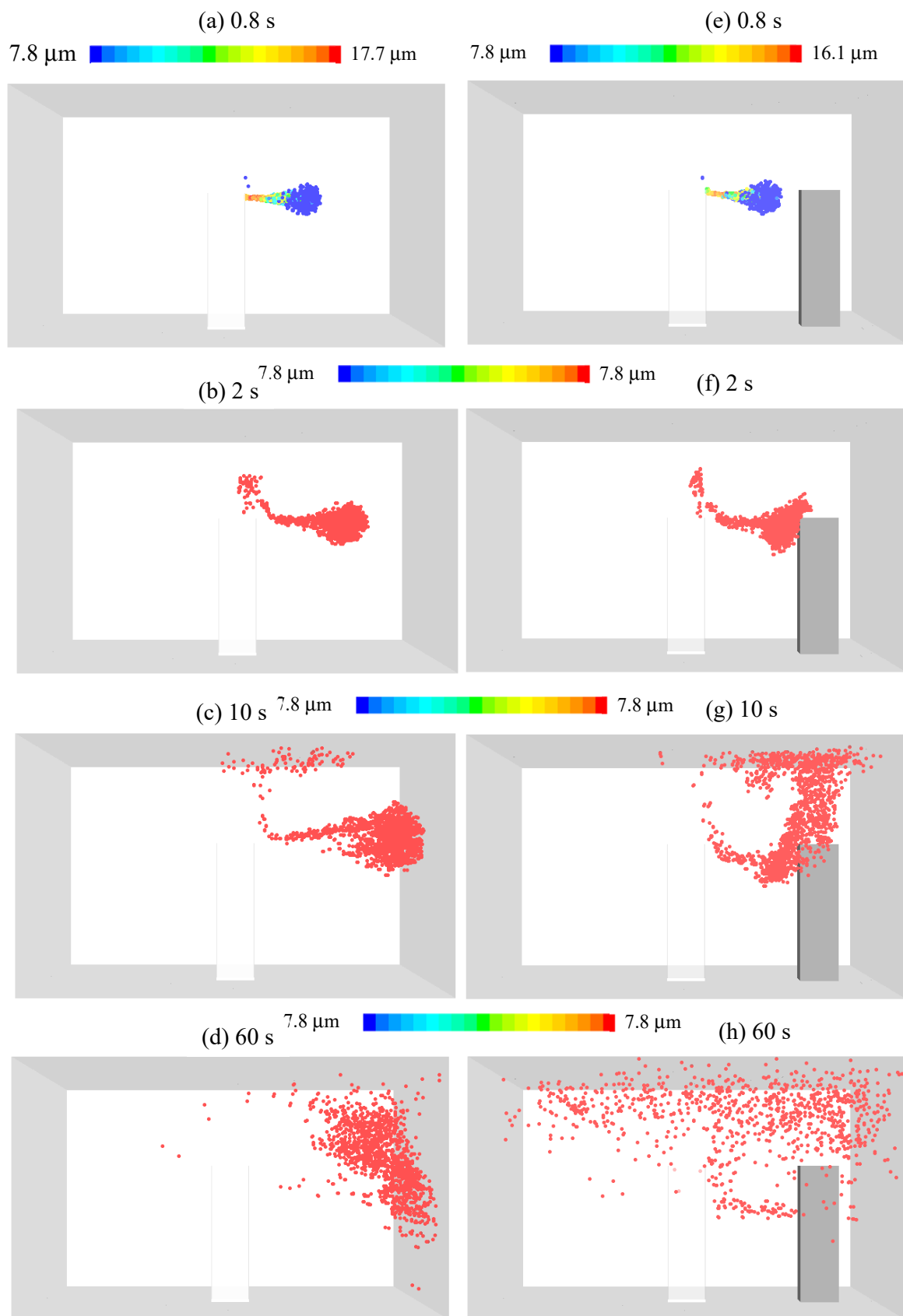


Figure 12. Droplet dispersion patterns for the case with one column (a–d) and the case with two columns (e–h).

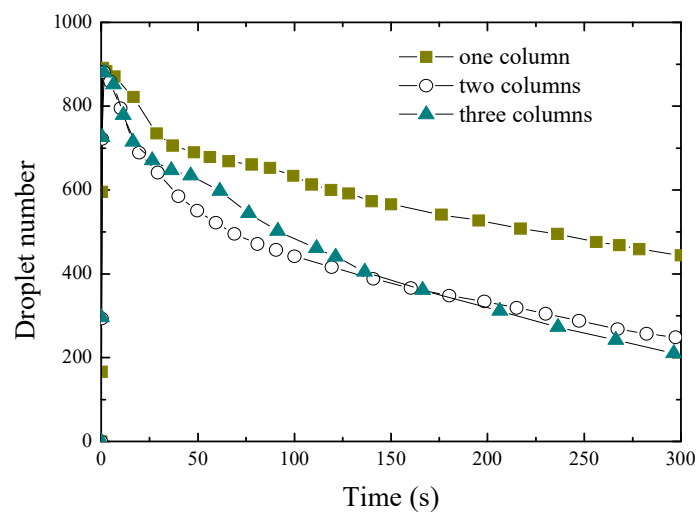


Figure 13. Number of droplets suspended in the air as a function of time.

Figure 12e–h show the droplet dispersion patterns when two persons stand in the room. At the moments of 0.8 s and 2 s; the droplet dispersion patterns are nearly not influenced by another person. After 2 s, the buoyancy-driven flow generated by another person significantly influences the droplet dispersion pattern. Many droplets migrate upward and disperse to the whole room at the moment of 60 s. Under this condition, droplets mainly suspend in the upper region of the room, which is different from the case with one person in the room. The number of droplets floating in the air is plotted in Figure 13. After 300 s, about 28% of the droplets are suspended in the air, indicating slow deposition. However, the number of droplets is less than that of the case with only one person, which indicates that many droplets are captured by the walls of the room due to the upward flow. The number of droplets suspended in the air for the case with three persons in the room (Figure 4c) is also shown in Figure 13 for comparison. Similar variation trends can be observed between the cases with two and three persons in the room. Hence, the number of persons in a room is a critical parameter in discussing the droplet dispersion behavior in a room.

5. Conclusions

The effect of buoyancy-driven flow on the migration of droplets generated by a coughing activity in a room was numerically discussed. The results demonstrated that a temperature stratification along the vertical direction occurred in the room and an umbrella-shaped airflow was generated by the warm column. For large droplets with an initial diameter of 100 μm , the flow in the boundary layer increased the deposition time (the time at which more than 99% of the droplets have been deposited on the walls of the room) by about five times. For small droplets with an initial diameter of 20 μm , the umbrella-shaped airflow resulted in a faster droplet dispersion and further resulted in faster droplet removal by the room walls. After 300 s, the suspended droplet number of the case with buoyancy-driven flow was 33.4% smaller than that of the case without buoyancy-driven flow. Two or three persons being in the room resulted in faster droplet removal. When an infected person stood in the room, droplets were mainly suspended in the downstream region of the cough flow. When two persons stood in the room, droplets were mainly suspended in the upper region of the room and the suspended droplet number was less than the case with only one person in the room. The number of suspended droplets in the case with three columns was nearly equal to that of the case with two columns.

Many human activities occur in the indoor environment and the buoyancy-driven flow is sensitive to the number, position, and shape of persons. The current study indicates the importance of the buoyancy-driven flow in the migration of respiratory droplets. In the future, the interactions between the buoyancy-driven flow and ventilation and various

respiratory activities require further research. In addition, the effect of the movement of the persons on droplet migration should be investigated in the future. The current study may guide the design of more efficient ventilation systems.

Author Contributions: Conceptualization, X.Y.; Methodology, X.Y.; Validation, N.L.; Investigation, N.L.; Writing—original draft, N.L.; Writing—review & editing, X.Y.; Supervision, X.Y.; Project administration, X.Y. All authors have read and agreed to the published version of the manuscript.

Funding: This research was funded by [Natural Science Basic Research Program of Shaanxi] grant number [Program No. 2022]Q-969].

Data Availability Statement: The data presented in this study are available on request from the corresponding author.

Acknowledgments: The authors greatly acknowledge the financial support from the Natural Science Basic Research Program of Shaanxi (Program No. 2022]Q-969).

Conflicts of Interest: The authors declare no conflict of interest.

References

1. Bazant, M.Z.; Bush, J.W.M. A guideline to limit indoor airborne transmission of COVID-19. *Proc. Natl. Acad. Sci. USA* **2021**, *118*, e2018995118. [[CrossRef](#)]
2. Wang, C.C.; Prather, K.A.; Sznitman, J.; Jimenez, J.L.; Lakdawala, S.S.; Tufekci, Z.; Marr, L.C. Airborne transmission of respiratory viruses. *Science* **2021**, *373*, 981. [[CrossRef](#)] [[PubMed](#)]
3. Abkarian, M.; Mendez, S.; Xue, N.; Yang, F.; Stone, H.A. Speech can produce jet-like transport relevant to asymptomatic spreading of virus. *Proc. Natl. Acad. Sci. USA* **2020**, *117*, 25237–25245. [[CrossRef](#)] [[PubMed](#)]
4. Chao, C.Y.H.; Wan, M.P.; Morawska, L.; Johnson, G.R.; Ristovski, Z.D.; Hargreaves, M.; Mengersen, K.; Corbett, S.; Li, Y.; Xie, X.; et al. Characterization of expiration air jets and droplet size distributions immediately at the mouth opening. *J. Aerosol Sci.* **2009**, *40*, 122–133. [[CrossRef](#)]
5. Han, Z.Y.; Weng, W.G.; Huang, Q.Y. Characterizations of particle size distribution of the droplets exhaled by sneeze. *J. R. Soc. Interface* **2013**, *10*, 20130560. [[CrossRef](#)]
6. Quiñones, J.J.; Doosttalab, A.; Sokolowski, S.; Voyles, R.M.; Castaño, V.; Zhang, L.T.; Castillo, L. Prediction of respiratory droplets evolution for safer academic facilities planning amid COVID-19 and future pandemics: A numerical approach. *J. Build. Eng.* **2022**, *54*, 104593. [[CrossRef](#)]
7. He, Q.; Niu, J.; Gao, N.; Zhu, T.; Wu, J. CFD study of exhaled droplet transmission between occupants under different ventilation strategies in a typical office room. *Build. Environ.* **2011**, *46*, 397–408. [[CrossRef](#)] [[PubMed](#)]
8. Lu, Y.; Lin, Z. Coughed droplet dispersion pattern in hospital ward under stratum ventilation. *Build. Environ.* **2021**, *208*, 108602. [[CrossRef](#)]
9. Das, S.K.; Alam, J.-E.; Plumari, S.; Greco, V. Transmission of airborne virus through sneezed and coughed droplets. *Phys. Fluids* **2020**, *32*, 097102. [[CrossRef](#)]
10. Yang, X.; Yang, H.; Ou, C.; Luo, Z.; Hang, J. Airborne transmission of pathogen-laden expiratory droplets in open outdoor space. *Sci. Total Environ.* **2021**, *773*, 145537. [[CrossRef](#)]
11. Rezaei, M.; Netz, R.R. Airborne virus transmission via respiratory droplets: Effects of droplet evaporation and sedimentation. *Curr. Opin. Colloid Interface Sci.* **2021**, *55*, 101471. [[CrossRef](#)]
12. Lieber, C.; Melekidis, S.; Koch, R.; Bauer, H.-J. Insights into the evaporation characteristics of saliva droplets and aerosols: Levitation experiments and numerical modeling. *J. Aerosol Sci.* **2021**, *154*, 105760. [[CrossRef](#)]
13. Liu, L.; Wei, J.; Li, Y.; Ooi, A. Evaporation and dispersion of respiratory droplets from coughing. *Indoor Air* **2016**, *27*, 179–190. [[CrossRef](#)] [[PubMed](#)]
14. Netz, R.R. Mechanisms of Airborne Infection via Evaporating and Sedimenting Droplets Produced by Speaking. *J. Phys. Chem. B* **2020**, *124*, 7093–7101. [[CrossRef](#)]
15. Bahramian, M.; Mohammadi, G. Ahmadi, Effect of indoor temperature on the velocity fields and airborne transmission of sneeze droplets: An experimental study and transient CFD modeling. *Sci. Total Environ.* **2023**, *858*, 159444. [[CrossRef](#)]
16. Pal, R.; Sarkar, S.; Mukhopadhyay, A. Influence of ambient conditions on evaporation and transport of respiratory droplets in indoor environment. *Int. Commun. Heat Mass Transf.* **2021**, *129*, 105750. [[CrossRef](#)]
17. Sheikhejad, Y.; Aghamolaei, R.; Fallahpour, M.; Motamedi, H.; Moshfeghi, M.; Mirzaei, P.A.; Bordbar, H. Airborne and aerosol pathogen transmission modeling of respiratory events in buildings: An overview of computational fluid dynamics. *Sustain. Cities Soc.* **2022**, *79*, 103704. [[CrossRef](#)]
18. Zhang, Z.; Chen, Q. Comparison of the Eulerian and Lagrangian methods for predicting particle transport in enclosed spaces. *Atmos. Environ.* **2007**, *41*, 5236–5248. [[CrossRef](#)]
19. Yu, H.; Mui, K.; Wong, L.; Chu, H. Ventilation of general hospital wards for mitigating infection risks of three kinds of viruses including Middle East respiratory syndrome coronavirus. *Indoor Built Environ.* **2016**, *26*, 514–527. [[CrossRef](#)]

20. Bogdan, A.; Ogłodziński, K.; Szyłak-Szydłowski, M. Analysis of thermal plumes forming over male human subjects. *J. Build. Eng.* **2022**, *45*, 103596. [[CrossRef](#)]
21. Hossain, M.; Chinenye-Kanu, N.; Faisal, N.H.; Prathuru, A.; Asim, T.; Banik, S. Numerical Prediction of the Effect of Thermal Plume of a Standing Human on the Airborne Aerosol Flow in a Room: Assessment of the Social Distancing Rule. *Aerosol Sci. Eng.* **2022**, *7*, 96–106. [[CrossRef](#)]
22. Sun, S.; Li, J.; Han, J. How human thermal plume influences near-human transport of respiratory droplets and airborne particles: A review. *Environ. Chem. Lett.* **2021**, *19*, 1971–1982. [[CrossRef](#)] [[PubMed](#)]
23. Wei, J.; Li, Y. Human Cough as a Two-Stage Jet and Its Role in Particle Transport. *PLoS ONE* **2017**, *12*, e0169235. [[CrossRef](#)] [[PubMed](#)]
24. Smolík, J.; Džumbová, L.; Schwarz, J.; Kulmala, M. Evaporation of ventilated water droplet: Connection between heat and mass transfer. *J. Aerosol Sci.* **2001**, *32*, 739–748. [[CrossRef](#)]
25. Tan, H.; Wong, K.Y.; Othman, M.H.D.; Kek, H.Y.; Nyakuma, B.B.; Ho, W.S.; Hashim, H.; Wahab, R.A.; Sheng, D.D.C.V.; Wahab, N.H.A.; et al. Why do ventilation strategies matter in controlling infectious airborne particles? A comprehensive numerical analysis in isolation ward. *Build. Environ.* **2023**, *231*, 110048. [[CrossRef](#)]
26. Jiang, Y.; Liu, G.; Ekambaram, P.; Yan, X. Lab-scale electrostatic droplet collection from a fog plume with droplet evaporation. *Appl. Therm. Eng.* **2023**, *223*, 120044. [[CrossRef](#)]
27. Akkus, Y. The effect of Stefan flow on the models of droplet evaporation. *J. Therm. Sci. Technol.* **2020**, *40*, 309–318. [[CrossRef](#)]
28. Morsi, S.A.; Alexander, A.J. An investigation of particle trajectories in two-phase flow systems. *J. Fluid Mech.* **1972**, *55*, 193–208. [[CrossRef](#)]
29. Ranz, W.E.; Marshall, W.R., Jr. Evaporation from drops, Part I. *Chem. Eng. Prog.* **1952**, *48*, 141–146.
30. Ranz, W.E.; Marshall, W.R., Jr. Evaporation from drops, Part II. *Chem. Eng. Prog.* **1952**, *48*, 173–180.
31. Tong, X.; Hong, S.W.; Zhao, L. CFD modelling of airflow pattern and thermal environment in a commercial manure-belt layer house with tunnel ventilation. *Biosyst. Eng.* **2019**, *178*, 275–293. [[CrossRef](#)]

Disclaimer/Publisher’s Note: The statements, opinions and data contained in all publications are solely those of the individual author(s) and contributor(s) and not of MDPI and/or the editor(s). MDPI and/or the editor(s) disclaim responsibility for any injury to people or property resulting from any ideas, methods, instructions or products referred to in the content.